A Compact Angular Rate Sensor System Using a Fully Decoupled Silicon-on-Glass MEMS Gyroscope

Said Emre Alper, Yuksel Temiz, and Tayfun Akin, *Member, IEEE*

***Abstract*—This paper presents the development of a compact single-axis angular rate sensor system employing a 100-μm-thick single-crystal silicon microelectromechanical systems gyroscope with an improved decoupling arrangement between the drive and sense modes. The improved decoupling arrangement of the gyroscope enhances the robustness of sensing frame against drive–mode oscillations and therefore minimizes mechanical crosstalk between the drive and sense modes, yielding a small bias instability. The gyroscope core element is fabricated by through-etching a 100-μm-thick silicon substrate which is anodically bonded to a recessed glass handling substrate. A patterned metal layer is included at the bottom of the silicon substrate, both as an etch-stop layer and a heat sink to prevent heating- and notching-based structural deformations encountered in deep dry etching in the silicon-on-glass process. The fabricated-gyroscope core element has capacitive actuation/sensing gaps of about 5 μm yielding an aspect ratio close to 20, providing a large differential sense capacitance of 18.2 pF in a relatively small footprint of 4.6 mm $\times$ 4.2 mm. Excitation and sensing electronics of the gyroscope are constructed using off-the-shelf integrated circuits and fit in a compact printed circuit board of size 54 mm $\times$ 24 mm. The complete angular rate sensor system is characterized in a vacuum ambient at a pressure of 5 mtorr and demonstrates a turn-on bias of less than 0.1 deg/s, bias instability of 14.3 deg/h, angle random walk better than 0.115 deg/$\sqrt{\text{h}}$, and a scale-factor nonlinearity of $\pm$0.6% in full-scale range of $\pm$50 deg/s. [2007-0158]**

***Index Terms*—Angular rate sensor, gyroscopes, quadrature coupling, silicon-on-glass (SOG) micromachining.**

I. Introduction

THE PROGRESS in micromachined or microelectromechanical systems (MEMS) vibratory gyroscopes enabled several newborn rate-grade applications starting in the early 1990s, where low cost and small size are essential, such as in the widespread automotive market [1], [2]. However, the performance of MEMS gyroscopes continuously increased within the past decade, approaching to the performance requirements of a number of military tactical-grade applications [3], [4]. It is expected that most of the tactical-grade applications will be dominated by micromachined inertial sensors by year 2020 [5]. One of the major limitations of the MEMS gyroscopes today is the mechanical cross-coupling between the drive and sense modes that arises due to poor manufacturing tolerances relative to the minimum feature size in micromachining technologies [6]. The amount of this coupling can be as high as 1000 deg/s [7]. Although it is possible to suppress the offset caused by unwanted mechanical coupling by more than two orders of magnitude using phase-sensitive detection, it still cannot be nulled completely and is still a dominant factor limiting the operating range, scale-factor linearity, and bias instability of MEMS gyroscopes [8]. As a numerical example, even a 1° phase error during the demodulation process causes 17-deg/s offset to appear at the gyroscope output due to a 1000-deg/s quadrature signal. A nondeterministic phase noise of 1 mdeg then causes an offset instability over 100 deg/h. Therefore, it can be concluded that any variation in the offset due to mechanical crosstalk directly exhibits a bias instability, and it is quite important to keep these unwanted crosstalk signals as small as possible.

There are various approaches reported for reducing mechanical coupling, including the use of electrostatic tuning [7]–[9], the drive electrode with 1-DOF motion [10], the sense electrode with 1-DOF motion [6], both the drive and sense electrodes with 1 DOF, and only the proof mass with 2 DOF [11]–[14]. Ideally, the sense electrodes must remain completely stationary during drive-mode oscillations for minimum bias instability, which is impractical since there should always be a physical connection between the drive-mode oscillator and the rate sensing frame in order to couple rotation-induced Coriolis forces acting on the oscillating mass to the sensing frame. This physical connection typically couples a significant portion of drive-mode oscillations to the sense-mode frame, depending on the mechanical design and fabrication tolerances. Other than the limitations due to fabrication tolerances, which can be optimized during the process development, there is still a need for increasing the structural immunity of the sense-mode frame against drive-mode oscillations in vibratory MEMS gyroscopes by properly arranging the movable frames and the flexures connecting those frames in order to minimize the amount of mechanical coupling.

This paper reports a new fully decoupled MEMS gyroscope with increased robustness of the sense-mode frames against drive-mode oscillations, and the construction of a high-performance yet compact angular rate sensor system using this new gyroscope as the core element. The MEMS gyroscope is fabricated with a specially developed fabrication process, in which a thin silicon substrate with a metal etch-stop layer at the bottom is anodically bonded to a glass substrate and patterned

Manuscript received July 4, 2007; revised September 27, 2008. Current version published December 4, 2008. This work was supported by the State Planning Organization (DPT) of Turkey. Subject Editor F. Ayazi.

S. E. Alper and T. Akin are with the Department of Electrical and Electronics Engineering, Middle East Technical University, Ankara 06531, Turkey (e-mail: said@metu.edu.tr; tayfun-akin@metu.edu.tr).

Y. Temiz was with the Department of Electrical and Electronics Engineering, Middle East Technical University, Ankara 06531, Turkey. He is now with the Institute of Electrical Engineering, Ecole Polytechnique Fédérale de Lausanne, 1015 Lausanne, Switzerland (e-mail: yuksel.temiz@epfl.ch).

Color versions of one or more of the figures in this paper are available online at http://ieeexplore.ieee.org.

Digital Object Identifier 10.1109/JMEMS.2008.2007274

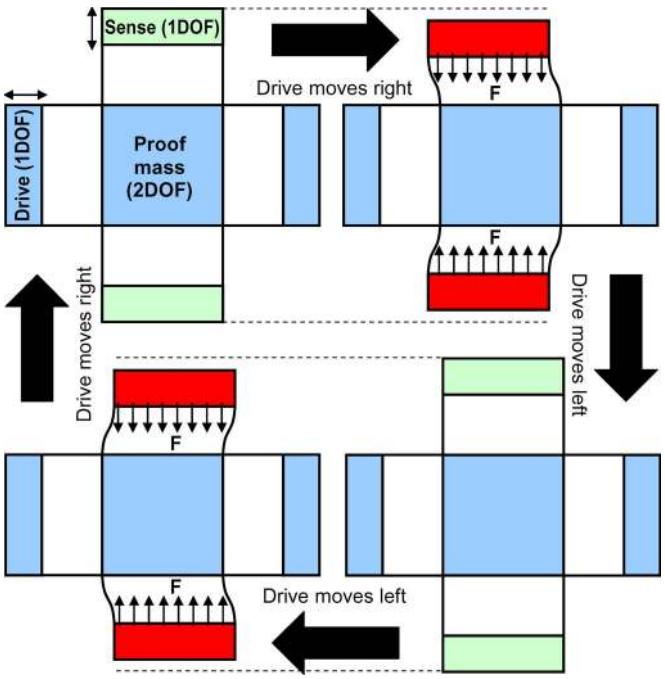

Fig. 1. Source for the frequency doubling at the sense mode. The sense-mode electrode is pulled down twice during the completion of a single cycle of drive-mode oscillations.

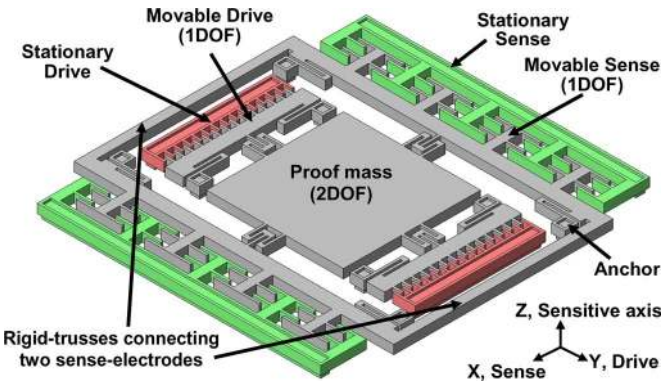

Fig. 2. Perspective view of the new fully decoupled gyroscope structure.

using deep reactive ion etching (DRIE). The process is optimized so that the fabricated silicon structures do not suffer from neither the notching nor heating effects experienced during DRIE, and the fabricated gyroscope has 100-μm-thick silicon structural layer with approximately 5-μm capacitive gaps. The gyroscope fabricated in this process is then used to construct a complete angular rate sensor system fitting into an area of only 13 cm^2, which demonstrates exceptional performance, even though discrete signal processing ICs are employed instead of a CMOS-ASIC. The measured performance of the angular rate sensor system is 14.3 deg/h and 6.9 (deg/h)/Hz$^{1/2}$ in terms of bias instability and white noise, respectively, which are currently limited by the electronics and not by the gyroscope core element. Section II describes the electromechanical design of the novel fully decoupled MEMS gyroscope, and Section III illustrates the new fabrication process eliminating the notching and heating effects associated with DRIE in silicon-on-glass (SOG) micromachining. Then, Section IV presents the characterization results of the MEMS gyroscope and the complete angular rate sensor system, and finally, Section V summarizes the conclusions of this paper.

II. Electromechanical Design

Electromechanical design is essential in minimizing the undesired mechanical crosstalk signals experienced in MEMS gyroscopes. One of the problems causing a nonzero mechanical crosstalk in the symmetric and decoupled gyroscopes of 1-DOF drive and 1-DOF sense frames is reported in [14], which states that there exists a time-varying signal at the sense electrode output with a frequency that is twice the drive-mode resonance frequency. Fig. 1 shows the source of this double-frequency motion, in which the sense-mode electrodes of the decoupled micromachined gyroscope structure are quasi-stationary during drive-mode oscillations, i.e., they do not move along the drive mode. However, drive-mode oscillations cause a spurious motion of the sense electrode along the sense-mode direction with a frequency that is twice that of drive-mode oscillations. This spurious double-frequency motion arises due to small but finite axial stresses induced in the flexible beams connecting the sense electrodes to the proof mass. Fortunately, the double-frequency motion causes a common-mode capacitance change at differential sense electrodes, which is partially suppressed by differential sensing. However, complete rejection of this double-frequency motion is only possible if the countermotion of each sense frame is identical, which is not possible due to mass imbalances during fabrication. Assuming that the differential sensing cannot reject even only 1% of this spurious double-frequency motion, and assuming that this motion propagates through the sense-mode demodulator with a 1° phase error (this phase error might be due to not only electronics but also the mechanical element itself even for a perfect second-order system), the resulting error at the output would be 175 ppm of the initial double-frequency motion. In other words, for a drive-mode vibration amplitude of 10 μm and a double-frequency motion of 0.2 μm, which is typical for sense frames without a rigid connection between them [14], the output offset signal due to the double-frequency motion would be 0.35 Å, corresponding to about 1 deg/s considering the sensor specifications. Any phase noise during demodulation may cause this offset to vary in time and add to bias instability of the gyroscope. Phase errors arise due to a number of factors, including stray capacitances across preamplifiers, frequency separation between the drive and sense modes, phase shift in the drive-mode automatic gain control electronics, etc. For a transresistance preamplifier circuit, for example, a 1-MΩ feedback resistance in parallel with a 100-fF stray capacitance results in 0.15° phase shift between the preamplifier input and output at 4 kHz. Phase errors can easily reach 1° with the contribution of the aforementioned factors and can increase bias instability together with spurious mechanical crosstalk. Therefore, minimizing the amount of any spurious motion, such as the double-frequency motion, has the potential to improve the bias stability of MEMS gyroscopes, which is considered in the new structure given hereinafter.

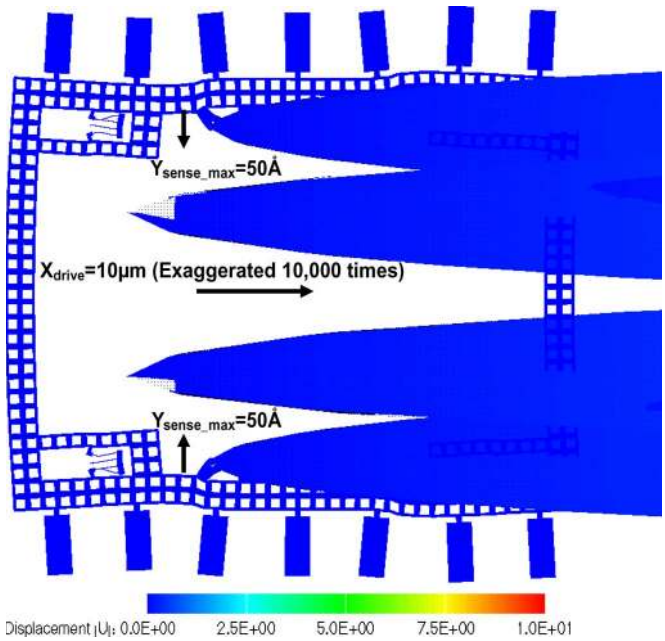

Fig. 3. Exaggerated visualization of the FEM simulation by CoventorWare, where the maximum displacement of the sense-mode frame of the designed MEMS gyroscope is less than 500 ppm of the drive-mode displacement.

Fig. 2 shows the perspective view of the new fully decoupled gyroscope structure. The new design preserves the major decoupling idea of previous designs [12]–[14], i.e., the drive and sense electrodes are restricted to 1-DOF motion for minimizing mechanical crosstalk, but now, the differential sense electrodes are mechanically connected to each other by rigid trusses constructing a single rectangular sense frame instead of two isolated bar-shaped sense frames. This way, the stiffness of the sense electrodes is highly increased against the spurious deflections caused by the oscillations along the drive mode. Constructing a rigid sense frame almost doubles the sense mass, i.e., reduces the Coriolis response by a factor of two. However, this reduction is acceptable considering the amount of suppression of the double-frequency motion and the increased immunity of the sense frames against rotary oscillations.

The amount of unwanted mechanical coupling of drive-mode oscillations to the sense frame is also analyzed by FEM simulations performed in the CoventorWare software. Fig. 3 shows the exaggerated visualization of the FEM simulation, where the maximum displacement of the sense-mode frame of the designed MEMS gyroscope is less than 500 ppm of the drive-mode displacement. This result correspond to an improvement by a factor of 40 compared to our previous work [13], [14], which does not have rigid sense frames. This would cause a mechanical crosstalk signal much less than 1 deg/s, when it is estimated for the 5.3-kHz matched-frequency operation, a drive-mode oscillation amplitude of 10 μm, and a sense-mode quality factor of 1000 at vacuum. This small mechanical signal can be further suppressed by differential reading as well as by phase-sensitive demodulation of the sense-mode output, leading to much better gyroscope stability.

The second problem that would increase mechanical crosstalk is the existence of unwanted oscillation modes with frequencies close to the operational frequency of the gyroscope.

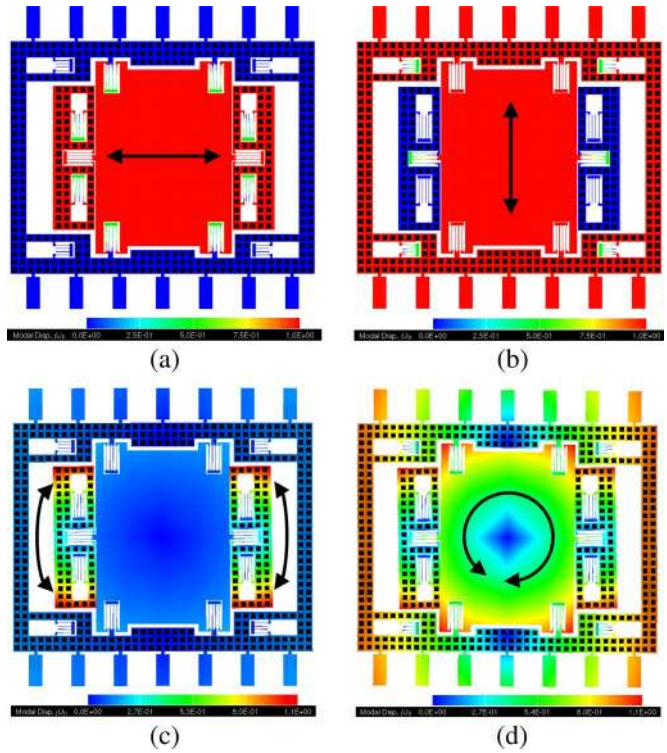

Fig. 4. First four mode shapes of the new gyroscope simulated by the CoventorWare FEM tool, including the drive and sense modes as well as the closest higher order modes.

TABLE I
RESONANCE FREQUENCIES ASSOCIATED WITH THE FIRST FOUR MODES OF SOG GYROSCOPE DESIGN

Mode	Resonance Frequency (Hz)
Drive	5,328
Sense	7,168
Rotary (drive-electrodes)	20,155
Rotary	22,436

Those modes can be excited by external physical inputs such as instant shocks and disturb the inherent operation. The high thickness (100 μm) of the proposed gyroscope sufficiently prevents any out-of-plane oscillation modes, and there remain only the in-plane rotary modes to be taken care of. For this reason, the flexures of the sense frame of the gyroscope are located in such a way that the sense frame is also highly robust against rotary oscillations that cause unwanted mechanical crosstalk between the operational modes and the higher order rotary modes.

Fig. 4 shows the first four mode shapes of the new gyroscope simulated by the CoventorWare FEM tool, including the drive and sense modes as well as the closest higher order modes. Table I provides the resonance frequencies associated with each mode. Increasing the rotational stiffness of the sense frame sufficiently separates the resonance frequencies of the higher order modes by about 15 kHz from the 5.3-kHz operational frequency of the gyroscope. In the predecessor [14] of this

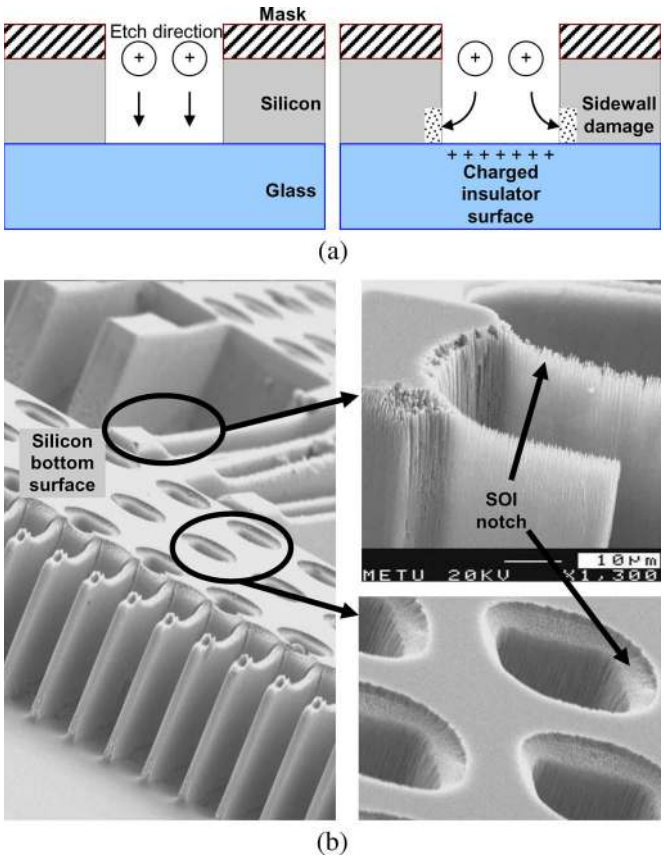

Fig. 5. (a) Mechanism of SOI notch and (b) resulting destruction at the bottom of a comb electrode array, a flexure beam, and an etch hole.

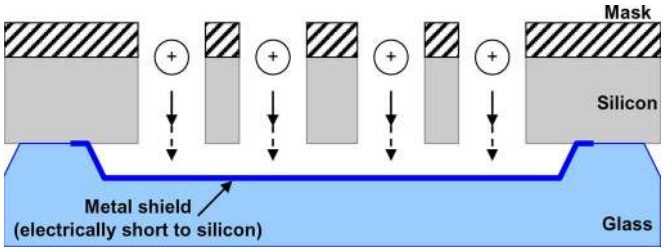

Fig. 6. Method to prevent SOI notch using a metal shield laid on the glass substrate under suspended silicon [17]. Here, the glass surface is not charged, and therefore, the directionality of ion bombardment does not change.

design, the frequency of the rotary mode was below the drive and sense resonance frequencies, and that of the out-of-plane mode was only 5 kHz above the operating frequency. With this new design, the unwanted mechanical coupling between the operational modes and the higher order modes is suppressed, ensuring a more stable operation.

III. SOG Fabrication Process

SOG micromachining is based on fabricating microstructures defined by through-etching of a thin silicon substrate anodically bonded to a machined glass substrate [4], [15]. Through-etching of the silicon substrate is usually performed by DRIE, for which aspect ratios higher than 30 are already reported [15]. The SOG micromachining process is appropriate for fabricating very thick and high-aspect-ratio silicon microstructures on low-loss insulating glass substrates, which yields highly sensitive capacitive inertial sensors with low mechanical–thermal noise and small parasitic capacitances.

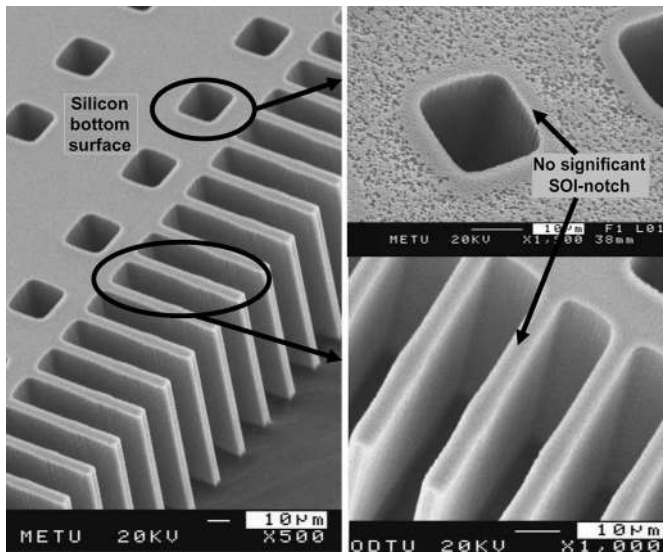

Fig. 7. SEM photographs of a comb electrode array of a gyroscope fabricated in the SOG process with the metal shield, showing the improvement achieved compared to Fig. 5.

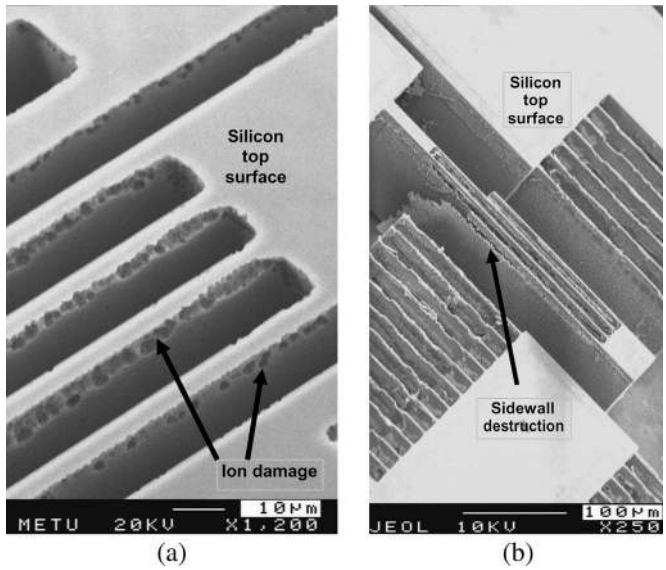

Fig. 8. SEM photographs of (a) ion damage and (b) resulting sidewall destruction in a narrow beam structure fabricated with the SOG process with the metal shield.

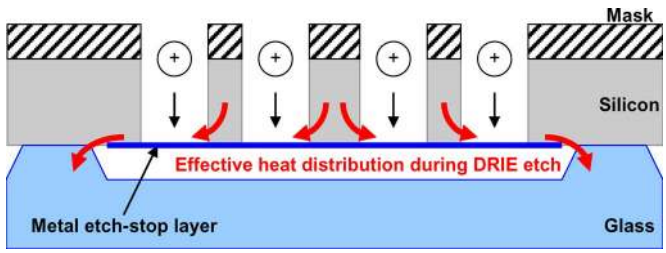

Fig. 9. New SOG process using a metal etch-stop layer to prevent SOI notch and silicon overheating problems simultaneously. It also prevents the release of microstructures during DRIE.

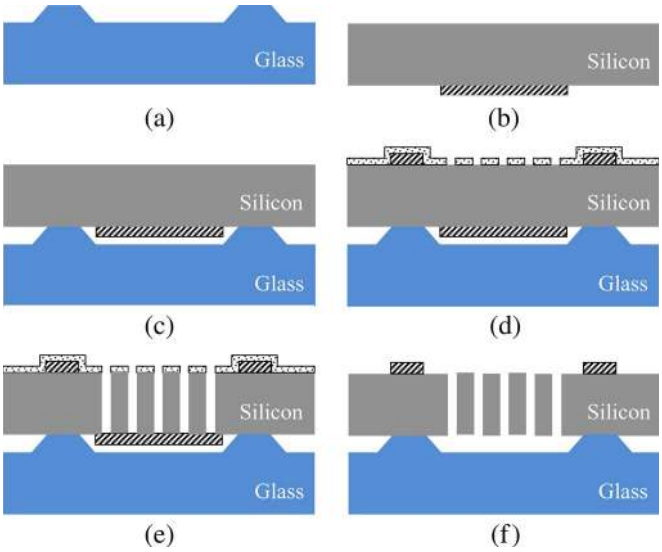

Fig. 10. New four-mask SOG fabrication process with the metal etch-stop layer used to implement the proposed gyroscope. (a) Form anchors on glass substrate. (b) Pattern Cr/Au shield at the bottom of the 100-μm-thick silicon substrate. (c) Anodic bonding of silicon and glass substrates. (d) Pattern pad metallization and the photoresist etch mask for DRIE. (e) Thoroughly etched silicon substrate until reaching the metal etch-stop layer. (f) Remove the metal etch-stop layer and then the photoresist etch mask.

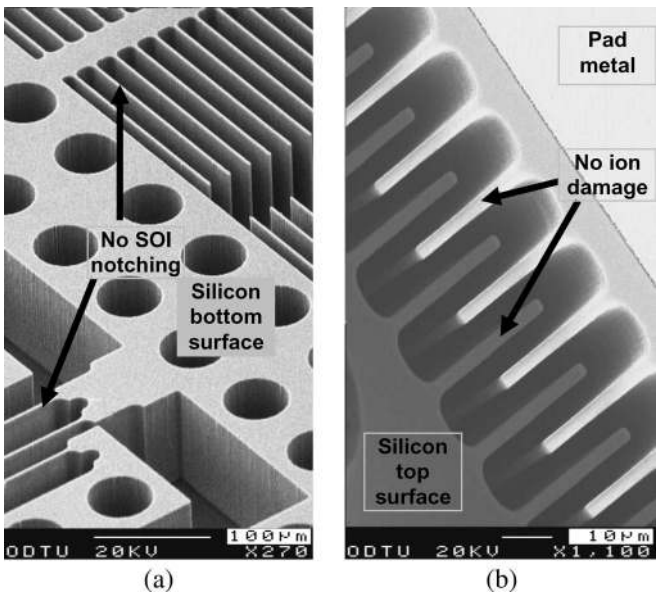

Fig. 11. SEM photographs of microstructures fabricated with the new SOG process with the metal etch-stop layer, (a) demonstrating no damage due to SOI notch at the bottom surface of the etched silicon for a comb electrode array, a flexure, and circular etch holes and (b) demonstrating no significant ion damage at the top surface of the etched silicon around a narrow comb finger array.

A major problem for through-wafer etch with DRIE is known as the aspect-ratio-dependent etching. This effect refers to the faster etch rate in a wide trench compared to the etch rate in a narrow trench. The effect of the etch-rate variation becomes essential for the through-etching of a silicon layer located on top of an insulating base. The ions passing through a completely etched cavity and reaching to the insulating base electrically charge the insulator surface, which can increase the charged potential to several tens of volts [16]. The successive ions are then deflected from the charged insulator surface to the

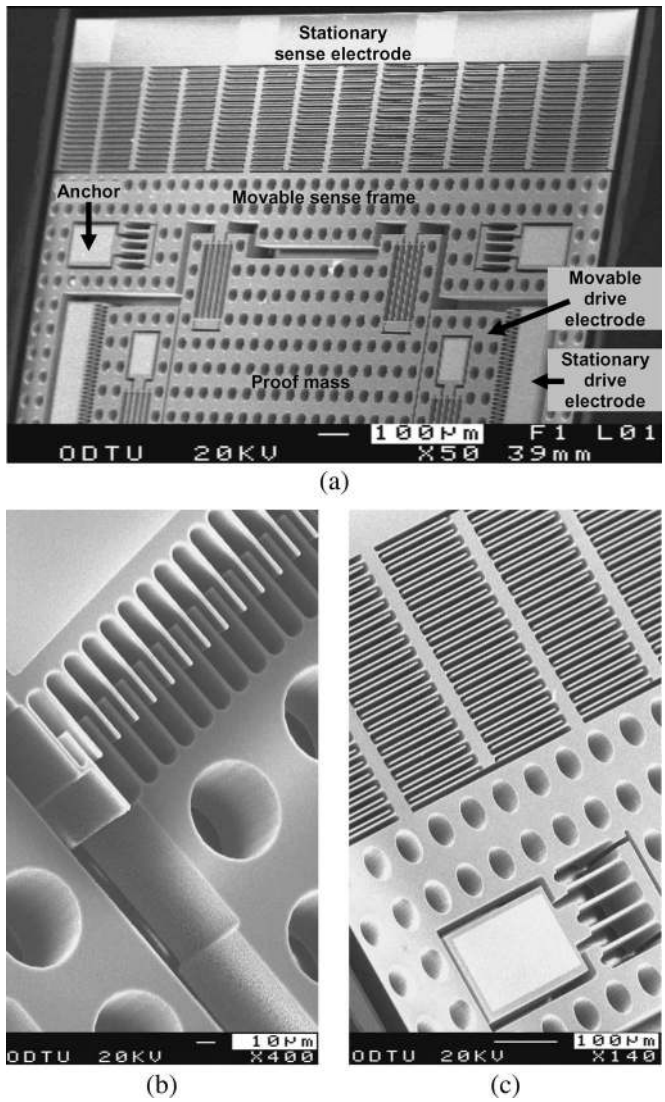

Fig. 12. SEM photographs of the fabricated SOG gyroscope. (a) Half of the symmetric structure. (b) Close-up view showing the varying-overlap-area-type drive combs. (c) Close-up view showing the varying-gap-type sense combs. The fabricated capacitive gaps are close to 5 μm, while the thickness of the structural silicon layer is 100 μm, yielding an aspect ratio of 20.

sidewalls of silicon trench, destroying the anisotropic nature of DRIE. This effect is called SOI notching and causes significant destruction of the etched microstructures if not taken care of. Fig. 5 describes the mechanism of SOI notch and shows the resulting destruction at the bottom of a comb electrode array, a flexure beam, and an etch hole.

Fig. 6 describes a method to prevent SOI notch using a metal shield laid on the glass substrate under suspended silicon [17]. The shield is extended inside the anchor regions, electrically shorting the metal shield to the etched silicon. As a result, ions passing through the fast-etched trenches are collected by the shield, and the glass surface remains uncharged. Therefore, no significant damage is observed in the etched silicon during excessive etch periods. Fig. 7 shows the SEM photographs of a comb electrode array of a gyroscope fabricated in the SOG process with the metal shield, showing the improvement achieved compared to Fig. 5.

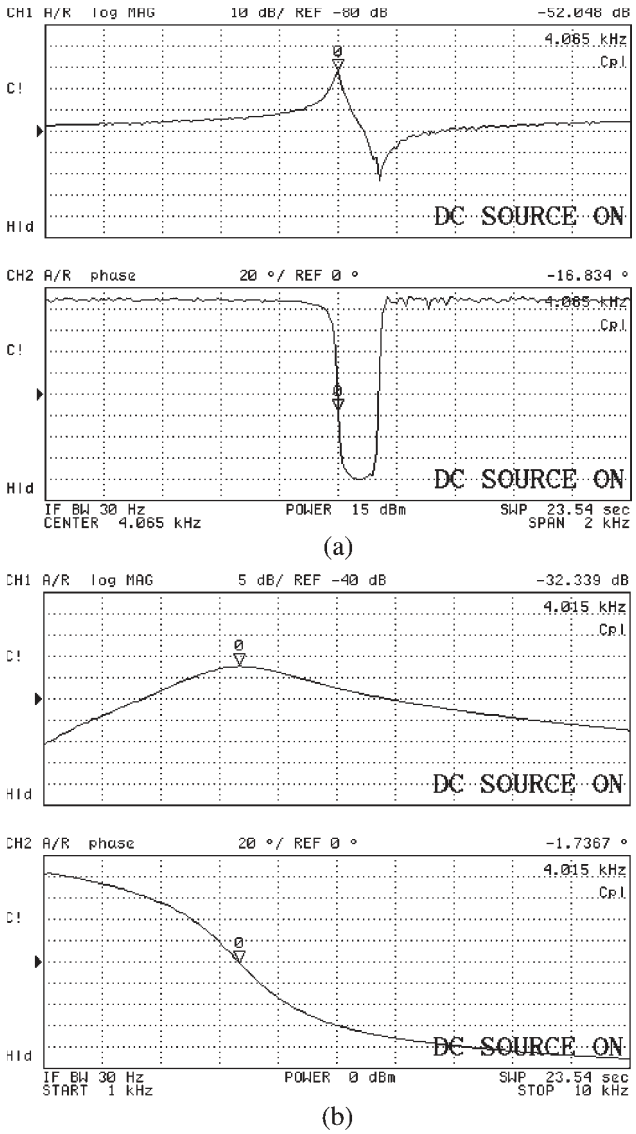

Fig. 13. Resonance characteristics for (a) the drive and (b) sense modes of the fabricated gyroscope measured using Agilent 4395A network analyzer and Karl Suss probe station.

Although the SOG process with the metal shield satisfactorily works in removing the SOI notch effect, it is experienced to be insufficient to prevent another detrimental effect observed in SOG processes, particularly when there are large suspended silicon masses with long thermal paths before reaching to the glass substrate. This is important since the silicon heats up during DRIE due to ion bombardment, and if this heat cannot be quickly transferred to the glass substrate under silicon, then both the etch rate and mask selectivity significantly reduce in the overheated silicon regions. The glass substrate can properly be cooled during DRIE, but the heat induced on the large suspended silicon structures can only be transferred to the cooled glass substrate through narrow silicon flexures, which are usually insufficient in heat transfer. Excessive heating of silicon causes photoresist mask erosion, and the sidewalls of narrow features are significantly thinned, if not completely etched. Fig. 8 shows the SEM photographs of (a) ion damage and (b) resulting sidewall destruction in a narrow beam structure fabricated with the SOG process with the metal shield.

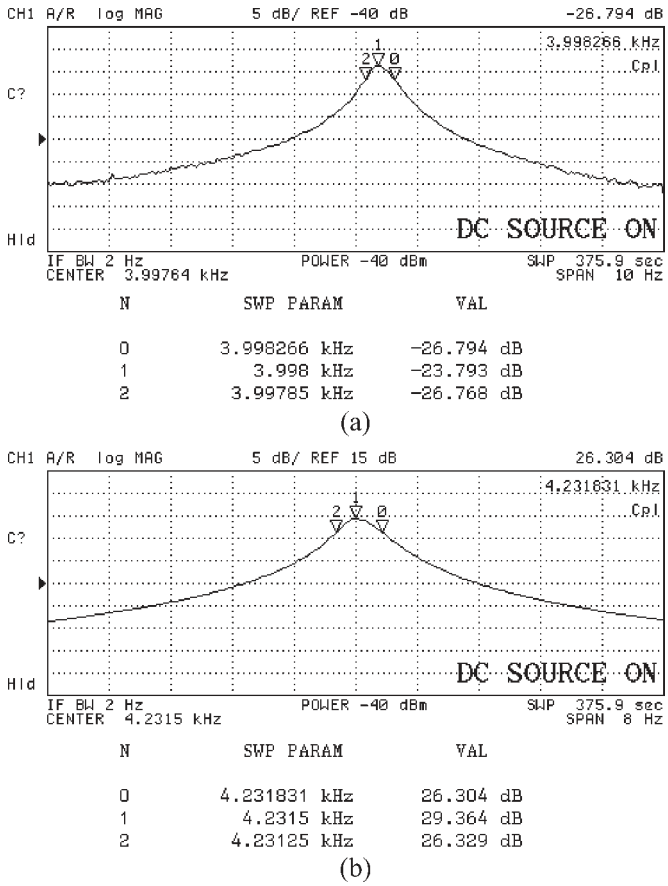

Fig. 14. Measured resonance characteristics of the gyroscope at 5-mtorr vacuum ambient, from which the quality factors of the (a) drive and (b) sense modes are extracted as 9611 and 7284, respectively.

The sidewall destruction problem in the SOG process a with metal shield is eliminated by using an advanced SOG process, for which the metal shield is laid directly at the bottom surface of the silicon substrate instead of the glass surface as in [18]. Now, the metal shield acts as a notch-preventing etch-stop layer as well as an efficient heat sink during DRIE. Fig. 9 shows the advantage of the new SOG process with the metal etch-stop layer. The use of metal shield also prevents the release of the suspended structures during DRIE; otherwise, the silicon structures are suspended and free to move once the silicon is thoroughly etched. This is also dangerous since the electrostatic forces between charged silicon frames will cause random movement of the suspended silicon before the completion of DRIE, which could easily destroy the narrow structures. In order to eliminate these problems, a new fabrication process is developed.

Fig. 10 shows the new four-mask SOG fabrication process with the metal etch-stop layer used to implement the proposed gyroscope. First, the anchor regions are defined by wet etch on a 500-μm-thick Pyrex glass substrate. Next, a Cr/Au etch-stop layer is patterned at the bottom side of a 100-μm-thick highly doped (111) silicon substrate. Then, the glass and silicon substrates are anodically bonded to each other. Finally, the silicon substrate is thoroughly etched with DRIE until the metal etch-stop layer, which prevents the SOI notch effect as well as the mask-erosion-based ion damage at the sidewalls of narrow

TABLE II
COMPARISON OF THE DESIGNED AND MEASURED ELECTROMECHANICAL PARAMETERS OF THE FABRICATED SOG GYROSCOPE

Parameter	Designed*		Measured	
	Drive	Sense	Drive	Sense
Capacitive gap, μm	5	5	5.3	5.6
Capacitance, fF	1.37	12.1	1.2	9.1
Mechanical resonance freq., Hz	3,644	5,041	4,065	Depends on V_{DC}
Voltage required for frequency matching, V_{DC}	-	28.8	-	31
Mechanical quality factor at atmospheric pressure	-	-	241	2,3
Mechanical quality factor at vacuum	-	-	9611	7284

* Takes into account a 2μm shrink/enlargement in feature/gap size due to undercut during DRIE.

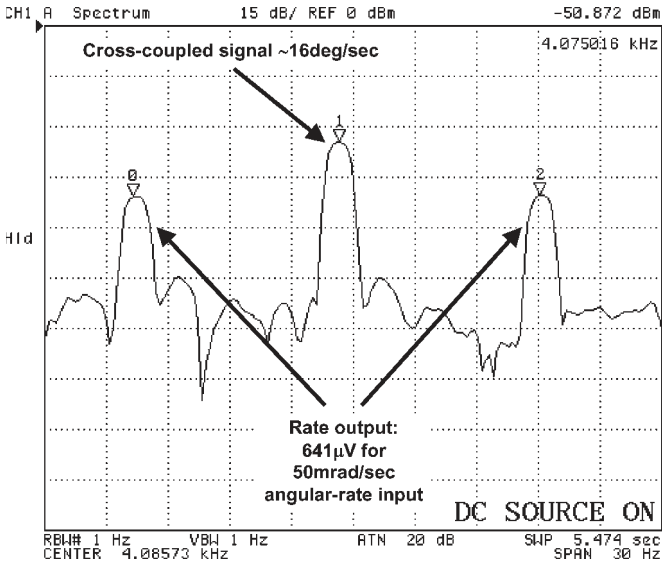

Fig. 15. Measured sense-mode raw output of the SOG gyroscope prior to demodulation, in response to a sinusoidal angular rate input having amplitude and frequency of 50 mrad/s (∼2.86 deg/s) and 10 Hz, respectively.

structures. Once the silicon etch is completed, the etch-stop metal layer is selectively etched in a wet etchant, while the pad metallization survives during this etch since it is still protected by the etch mask of DRIE, as shown in Fig. 10(e). Following the removal of the metal etch-stop layer, the etch mask of DRIE is also removed in wet stripping solution, and the structures are released by drying on a hot plate after alcohol rinse. The high stiffness of the 100-μm-thick silicon layer eliminates the risk of stiction during this release process.

Fig. 11 shows the SEM photographs of microstructures fabricated with the new SOG process with the metal etch-stop layer, (a) demonstrating no damage due to SOI notch at the bottom surface of the etched silicon for a comb electrode array, a flexure, and circular etch holes and (b) demonstrating no significant ion damage at the top surface of the etched silicon around a narrow comb finger array. Fig. 12 shows the SEM photographs of the fabricated SOG gyroscope. The fabricated gyroscope has a differential sense electrode capacitance of 18.2 pF within a footprint less than 20 mm^2, owing to the 100-μm structural layer thickness etched with an aspect ratio close to 20, yielding an average of 5.5-μm capacitive gaps.

IV. CHARACTERIZATION RESULTS

The capacitances of a single set (half of differential) of drive and sense electrodes of the fabricated gyroscope are measured using Agilent 4294A precision impedance analyzer as 1.2 and 9.1 pF, respectively. These values are slightly smaller than the design values of 1.4 and 12.1 pF, respectively, which also include the simulated electrostatic fringe-field correction factors. This small mismatch is possibly due to the enlarged capacitive gaps of the fabricated gyroscope, which cause a reduction in both the parallel-plate capacitors and the fringe-field correction factors. The fabricated capacitive gaps are 5.3 and 5.6 μm for the drive and sense electrodes, respectively, which are slightly different from each other and from the layout value of 5 μm, basically due to the mask-dependent etch variations in DRIE.

Fig. 13 shows the resonance characteristics for the drive and sense modes of the fabricated gyroscope measured with Agilent 4395A network analyzer and Karl Suss probe station. The sense-mode resonance frequency can be tuned down to 50 Hz below the drive-mode frequency of 4.065 kHz with a dc polarization voltage of 31 V applied to the proof mass. The measured drive- and sense-mode mechanical resonance frequencies and the polarization voltage required for frequency matching are both close to the expected values of 3.64 kHz and 28.8 V, respectively, estimated for a DRIE undercut of 2 μm around narrow flexures during 100-μm-deep etch.

The quality factors of the SOG gyroscope for the drive and sense modes at atmospheric pressure are measured to be 241 and 2.3, respectively. The large etch holes on the perforated masses and the high-aspect-ratio sense fingers result in small quality factors at atmosphere; however, the gyroscope performance significantly improves at vacuum for which the air damping becomes negligible. Fig. 14 shows the measured resonance characteristics of the gyroscope at

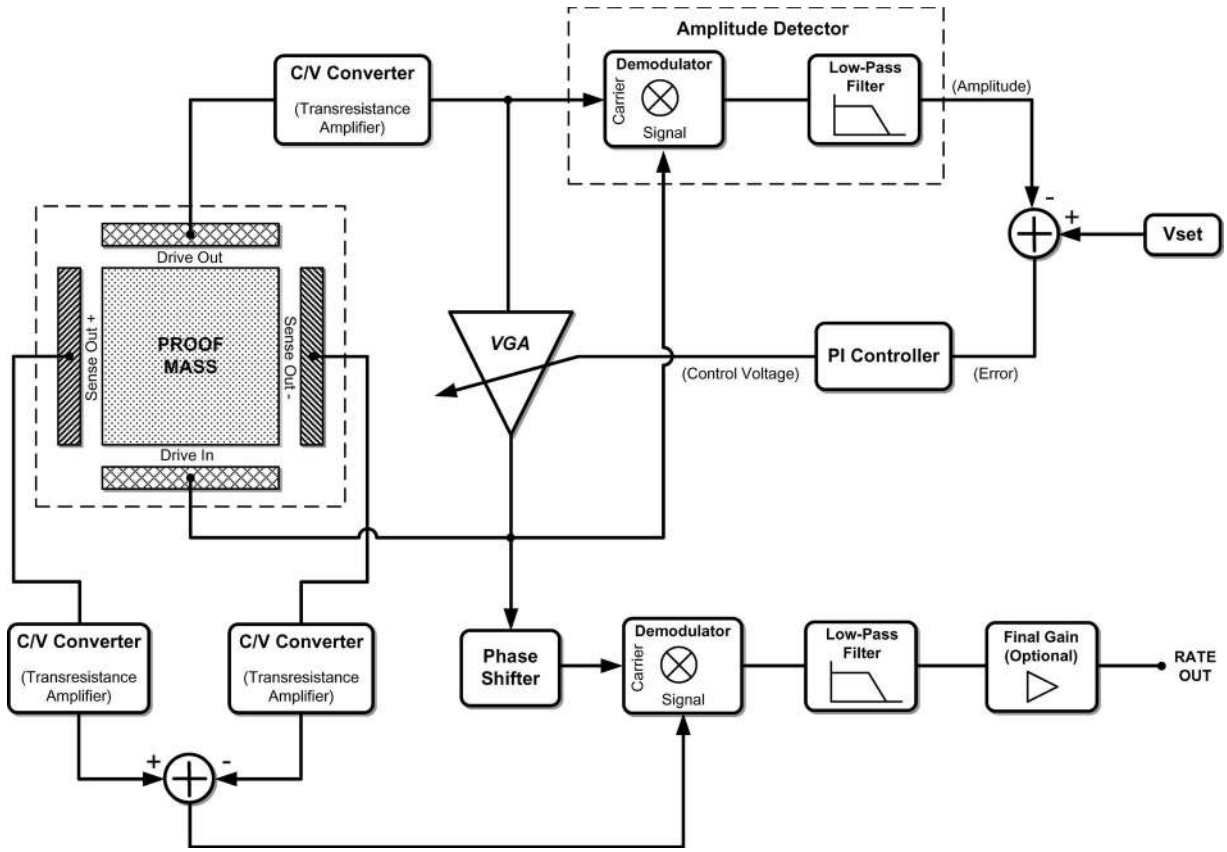

Fig. 16. Block diagram of the complete angular rate sensor system.

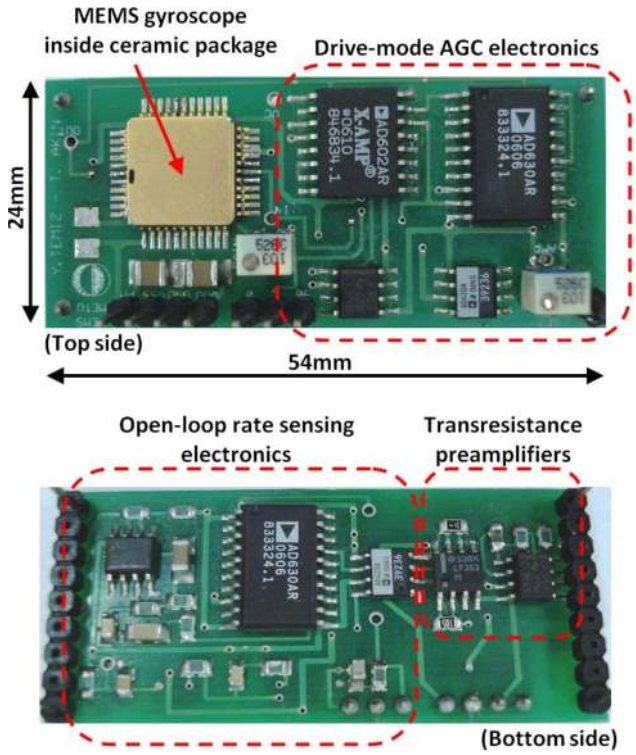

Fig. 17. Compact PCB of the complete angular rate sensor system, fitting into an area less than 13 cm^2.

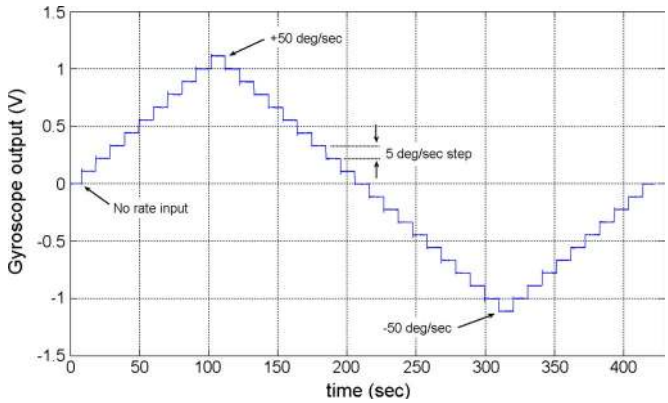

Fig. 18. Measured response of the angular rate sensor starting from zero rate, first reaching up to 50 deg/s, next reaching down to −50 deg/s, and finally reaching up to zero rate again, using 5-deg/s steps during the test.

5-mtorr vacuum ambient, from which the quality factors of the drive and sense modes are extracted as 9611 and 7284, respectively. The high quality factor does not cause any comb-instability problems in the drive mode due to the very high (> 100-kN/m) axial stiffness of the drive-mode flexures along the sense direction. Table II provides a comparison of the designed and measured electromechanical parameters of the fabricated SOG gyroscope.

Fig. 15 shows the sense-mode raw output of the SOG gyroscope prior to demodulation, in response to a sinusoidal angular rate input having amplitude and frequency of 50 mrad/s (∼2.86 deg/s) and 10 Hz, respectively. The central peak in this response corresponds to the sum of the quadrature and in-phase coupling signals from the drive mode to the sense output. The sidelobes correspond to the raw sense output signals, which are separated from the central peak by the frequency of the

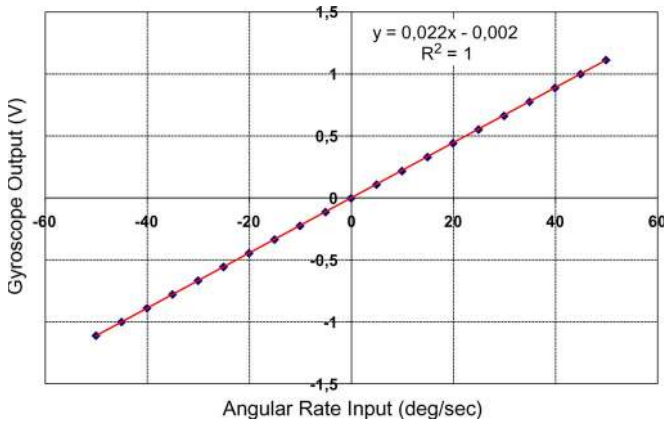

Fig. 19. Measured response curve of the fabricated angular rate sensor system specifying the scale factor, the zero-rate offset, and the nonlinearity.

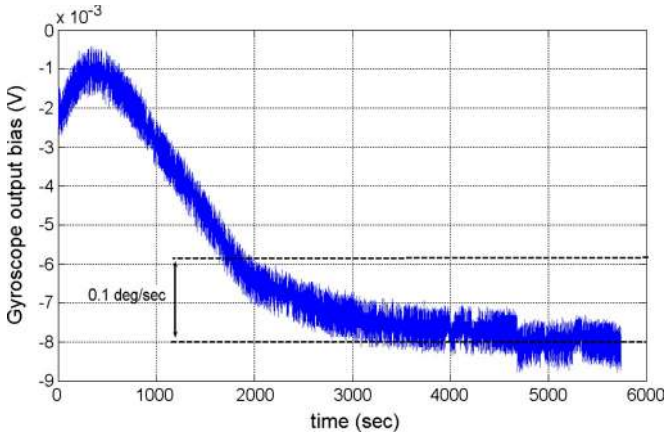

Fig. 20. Bias drift data collected from the rate output, while the sensor is located in the vacuum chamber and kept stationary during the test.

applied angular rate input, i.e., 10 Hz. The separation between the drive- and sense-mode resonance frequencies is approximately 200 Hz for the near-match-mode operation, which is sufficiently high to prevent any imbalance between the amplitudes of the sidelobes that are ± 10 Hz separated from the drive-mode resonance frequency. The mechanical rate sensitivity of the gyroscope is about 224 μV_{rms}/(deg/s), while the measured sum of quadrature and in-phase coupling signals is approximately 3.6 mV_{rms}, corresponding to a rate-equivalent coupling of only 16 deg/s. Quadrature coupling is believed to dominate this value since the measured turn-on bias of the gyroscope, which has been directly affected by the in-phase coupling that cannot be filtered out by demodulation, is on the order of 0.1 deg/s. The measured quadrature signal is quite small compared to the values in our previous work [14] and in some other studies reported in the literature [6]–[8]. It should be noted that the measured noise level in the raw sensor output has been observed to be significantly increased by the rate table servomotor; therefore, it is not suitable to predict the noise-equivalent rate from Fig. 15.

In order to construct a fully functional angular rate sensor system, the fabricated MEMS gyroscope is first wirebonded to a surface-mount ceramic package and then integrated with signal processing electronic circuitry on a compact printed circuit board. Fig. 16 shows the block diagram of the complete angular rate sensor system. Most part of the system aims the generation and control of stable drive-mode oscillations using closed-loop control techniques. The preamplifier stage is a capacitance-to-voltage converter, and it is used together with the variable-gain amplifier (VGA) to satisfy the phase requirements for starting self-oscillations along the drive mode of the gyroscope. The amplitude of this oscillation is controlled by referencing the measured drive-mode oscillation amplitude to a desired amplitude signal (Vset) and then by minimizing the error between these signals using a proportional–integral (PI) controller. The output of the PI controller continuously adjusts the gain of VGA in order to keep the drive-mode oscillation amplitude constant at the desired level. Once a stable drive-mode oscillation is achieved, the system is ready for angular rate measurements. The open-loop rate sensing mechanism of the system is straightforward: Differential sense outputs picked by identical transresistance preamplifier stages are converted to a single-ended signal using an instrumentation amplifier, demodulated by using phase-sensitive demodulation with a carrier signal generated from drive-mode oscillations, and low-pass filtered to provide a dc output that is proportional to the applied angular rate input signal. An optional gain stage provides the calibration of the scale factor, which is typically not needed for the SOG gyroscope used in this prototype system. Fig. 17 shows the compact PCB of the complete angular rate sensor system, fitting into an area less than 13 cm^2, which is comparable to similar high-performance MEMS gyroscopes with discrete IC electronics [19]. The lid of the surface-mount ceramic package is not hermetically sealed, allowing sensor characterization in a vacuum chamber. In an application environment, the vacuum packaging of the gyroscope can be achieved on ceramic package level or in wafer level [20].

The complete angular rate sensor system is tested in a vacuum chamber mounted on the Ideal Aerosmith 1280 VS single-axis rate table. The chamber is vacuumed down to 5 mtorr using a mechanical pump to characterize the zero-rate bias, scale factor, bias instability, and angle random walk of the sensor. For the characterization of the gyroscope at vacuum, it is quite difficult to keep the drive- and sense-mode resonance frequencies matched against temperature variations without closed-loop control. Therefore, a dc polarization voltage of 30 V is applied to the gyroscope, operating it with near-match drive and sense frequencies. Fig. 18 shows the measured response of the angular rate sensor starting from zero rate, first reaching up to 50 deg/s, next reaching down to -50 deg/s, and finally reaching up to zero rate again, using 5-deg/s steps during the test. Fig. 19 shows the measured input rate versus dc output voltage response of the fabricated angular rate sensor system specifying the calibrated scale factor, the zero-rate offset, and the nonlinearity. The sensor has a scale factor of 22.2 mV/(deg/s) with a zero-rate offset of 2.2 mV, corresponding to 0.1 deg/s. The offset is pretty small due to phase-sensitive demodulation as well as the small mechanical coupling between the drive and sense modes of the new MEMS gyroscope. The measured quadrature coupling of 16 deg/s and a null bias of 0.1 deg/s correspond to a demodulation phase error of 0.36°, which is expected to be reduced if a dedicated ASIC chip were

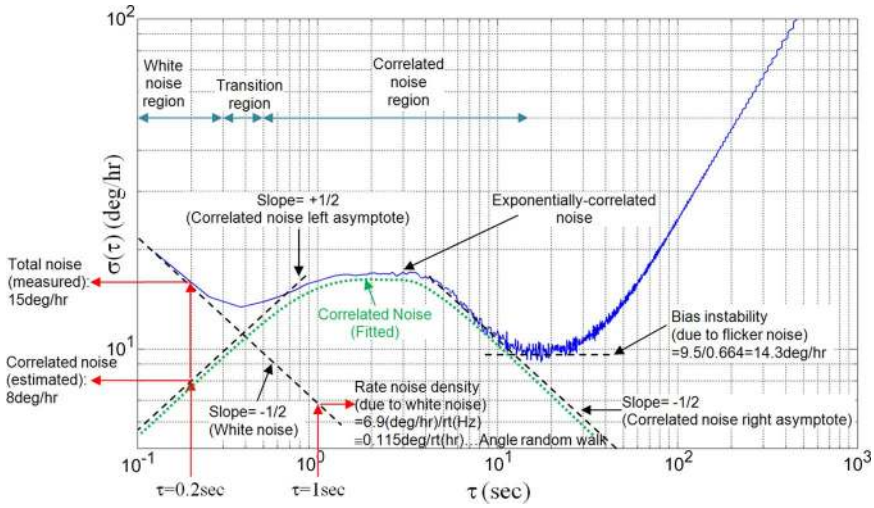

Fig. 21. Allan variance plot of the fabricated gyroscope, obtained by processing the measured drift data of Fig. 20.

used instead of PCB-level electronics. Another important performance figure of the characterized angular rate sensor system is the linearity of the scale factor. The R^2-nonlinearity of the data of Fig. 19 is measured to be less than $\pm 0.01\%$, whereas the composite nonlinearity of the scale factor (including hysteresis, systematic nonlinearity, and other uncertainties in the measurement) is measured to be as low as $\pm 0.6\%$, i.e., compatible with several commercial rate sensors [19]–[21]. The measurement range of the angular rate sensor system is currently limited to ± 50 deg/s, above which the scale-factor nonlinearity increases significantly due to open-loop rate sensing.

The Allan variance analysis is used in order to determine the bias instability and angle random walk of the fabricated angular rate sensor system [22]. The output of the sensor is collected for a period of more than 1.5 h, which is observed to be sufficient for determining the bias instability and angle random walk of the gyroscope. Fig. 20 shows the bias drift data collected from the rate output, while the sensor is located in the vacuum chamber and kept stationary during the test. The initial bias trend shows an overshoot at the beginning of the test, but it drops to 0.025 (deg/s)/h after about 1 h. We believe that this characteristic is due to the thermal stabilization of the system and can be easily modeled and compensated by external electronics. Fig. 21 shows the Allan variance plot of the fabricated gyroscope, which is obtained by processing the measured drift data of Fig. 20. The possible reason for having a plot with two dips is due to the exponentially correlated noise, as explained in [22]. The potential source of the exponentially correlated noise is reported to be the randomized dither vibrations in ring-laser gyros [23] or similar phenomena observed in spinning-wheel gyros [22]. We believe that randomized environmental vibrations caused by the vacuum pump located in close vicinity of the rate table also generate a similar exponentially correlated noise (as in Fig. 21). The bias stability (due to flicker noise) of the gyroscope is found by dividing the measured dip level of the Allan variance plot of Fig. 21 by a factor of 0.664, as described in [22], which yields 14.3 deg/h. The measured amount of bias stability is not affected by the initial thermal stabilization characteristics, since the time constant of thermal stabilization is about 1000 s, which is much higher than the averaging time of 15 s for reaching the bias instability limit. The bias stability of the sensor is believed to be limited by open-loop sense electronics, the measurement setup inside the vacuum chamber under continuous pumping, and the stability of the proof mass voltage.

The plot of Fig. 21 can also be used to specify the angle random walk (due to white noise) of the developed angular rate sensor system. Rate noise density due to white noise can be represented by fitting a line with slope $-1/2$ to the region of the Allan variance plot, for which the measured data can be well represented by the fit line [22]. The rate noise density can then be directly obtained by reading this fit line at $\tau = 1$ s, which yields 6.9(deg/h)/Hz$^{1/2}$ or, equivalently, an angle random walk of 0.115 deg/h$^{1/2}$. The accuracy of this measurement is also examined against the fact that whether the correlated noise is affecting the correct measurement of angle random walk or not. The correlated noise can be modeled by fitting two asymptotes to the Allan variance graph with slopes of $\pm 1/2$, as described in [22]. The contributions of correlated noise and white noise in the total measured noise are then found to be 8 and 12.7 deg/h, respectively, for a sampling time of $\tau = 0.2$ s (or a sampling frequency of 5 Hz), verifying that the selected sampling time is dominated by the white-noise power. The white-noise density in 1-Hz bandwidth can then be calculated as 5.7 deg/h or, equivalently, 5.7(deg/h)/Hz$^{1/2}$. This value is 18% less and even better than the value that is directly obtained from the fit line that describes white noise. This analysis shows that the existence of correlated noise in the Allan variance plot does not prevent the determination of angle random walk with an acceptable accuracy. The measured angle random walk is believed to be sufficiently low, considering that the whole electronic stages, including preamplifiers, are constructed by discrete ICs and passive components.

The developed angular rate sensor system demonstrates an exceptional performance by integrating a novel fully decoupled MEMS gyroscope with high-quality electronics generating amplitude-controlled stable drive-mode oscillations and extracting the rate signal by phase-sensitive detection. The integrated system occupies a compact size, which improves reliability and repeatability.

V. Conclusion

This paper presents the design and fabrication of a 100-μm-thick single-crystal silicon MEMS gyroscope with an improved decoupling arrangement between the drive and sense modes, where the gyroscope is used in the development of a compact single-axis angular rate sensor system. The improved decoupling arrangement is achieved by a special arrangement of sense-mode frame and flexures, minimizing both double-frequency mechanical crosstalk and quadrature signal, which are the two important effects limiting the stability of MEMS gyroscopes. The gyroscope is fabricated by using DRIE and through-wafer etching of a 100-μm-thick silicon substrate which is anodically bonded to a glass substrate; the notching and heating effects associated with DRIE of silicon are eliminated by using a sacrificial metal etch-stop layer patterned at the bottom of the thin silicon substrate. The fabricated gyroscope has capacitive gaps of about 5 μm yielding an aspect ratio close to 20, which results in a total differential sense capacitance of 18.2 pF in a footprint of 4.2 mm $\times$ 4.6 mm. The fabricated MEMS gyroscope is then integrated with drive-mode automatic gain control and sense-mode signal processing electronics, all fitting on a PCB of area less than 13 cm^2. The complete angular rate sensor system is then characterized at vacuum, and it is shown that the system demonstrates a scale factor of 22.2 mV/(deg/s), with a composite nonlinearity as small as $\pm 0.6\%$ within the $\pm$50-deg/s measurement range. The zero-rate bias of the sensor is less than 0.1 deg/s after turn-on, while the bias instability is measured to be only 14.3 deg/h. The rate-equivalent white-noise density of the gyroscope is measured to be better than 6.9(deg/h)/Hz$^{1/2}$, although all of the electronic stages are constructed by discrete ICs and passive components. The performance of the developed sensor system can be extended further by using closed-loop rate sensing electronics and hermetically sealing the sensor in a package with stable vacuum inside.

References

[1] K. Funk, H. Emmerich, A. Schilp, M. Offenberg, R. Neul, and F. Larmer, "A surface micromachined silicon gyroscope using a thick polysilicon layer," in *Proc. 12th IEEE Int. Conf. MEMS*, Orlando, FL, Jan. 1999, pp. 57–60.

[2] S. Chang, M. Chia, P. Castillo-Borelley, W. Hidgon, Q. Jiang, J. Johnson, L. Obedier, M. Putty, Q. Shi, D. Sparks, and S. Zarabadi, "An electroformed CMOS integrated angular rate sensor," *Sens. Actuators A, Phys.*, vol. 66, no. 1–3, pp. 138–143, Apr. 1998.

[3] M. Weinberg, J. Connely, A. Kourepenis, and D. Sargent, "Microelectromechanical instrument and systems development at the Charles Stark Draper Laboratory," in *Proc. AIAA/IEEE Digital Avionics Syst. Conf.*, Oct. 1997, pp. 8.5.33–8.5.40.

[4] G. He and K. Najafi, "A single-crystal silicon vibrating ring gyroscope," in *Proc. 15th IEEE Int. Conf. MEMS*, Las Vegas, NV, Jan. 2002, pp. 718–721.

[5] G. T. Schmidt, "INS/GPS technology trends," in *Proc. NATO RTO Sens. Electron. Technol. (RTO-SET) Panel: Symp. Emerging Mil. Capabilities Enabled Advances Navigat. Sens. (SET)*, Istanbul, Turkey, Oct. 2002, pp. 55–62.

[6] J. A. Geen, S. J. Sherman, J. F. Chang, and S. R. Lewis, "Single-chip surface micromachined integrated gyroscope with 50°/h Allan deviation," *IEEE J. Solid-State Circuits*, vol. 37, no. 12, pp. 1860–1866, Dec. 2002.

[7] W. A. Clark, R. T. Howe, and R. Horowitz, "Surface micromachined Z-axis vibratory rate gyroscope," in *Proc. Solid-State Sens. Actuator Workshop*, Hilton Head, CA, Jun. 2–6, 1996, pp. 283–289.

[8] M. Palaniapan, R. T. Howe, and J. Yasaitis, "Performance comparison of integrated Z-axis frame microgyroscopes," in *Proc. 16th IEEE MEMS Workshop*, Kyoto, Japan, Jan. 2003, pp. 482–485.

[9] F. Ayazi and K. Najafi, "A HARPSS polysilicon vibrating ring gyroscope," *J. Microelectromech. Syst.*, vol. 10, no. 2, pp. 169–179, Jun. 2001.

[10] W. Geiger, W. U. Butt, A. Gaißer, J. Frech, M. Braxmaier, T. Link, A. Kohne, P. Nommensen, H. Sandmaier, and W. Lang, "Decoupled microgyros and the design principle DAVED," *Sens. Actuators A, Phys.*, vol. 95, no. 2/3, pp. 239–249, Jan. 2002.

[11] M. S. Kranz and G. K. Fedder, "Micromechanical vibratory rate gyroscopes fabricated in conventional CMOS," in *Proc. Symp. Gyro Technol.*, 1997, pp. 3.0–3.8.

[12] S. E. Alper and T. Akin, "Symmetrical and decoupled nickel microgyroscope on insulating substrate," *Sens. Actuators A, Phys.*, vol. 115, no. 2/3, pp. 336–350, Sep. 2004.

[13] S. E. Alper and T. Akin, "A single-crystal silicon symmetrical and decoupled MEMS gyroscope on an insulating substrate," *J. Microelectromech. Syst.*, vol. 14, no. 4, pp. 707–717, Aug. 2005.

[14] S. E. Alper, K. Azgin, and T. Akin, "High-performance SOI-MEMS gyroscope with decoupled oscillation modes," in *Proc. 19th IEEE Int. Conf. MEMS*, Istanbul, Turkey, Jan. 22–26, 2005, pp. 70–73.

[15] J. Chae, H. Kulah, and K. Najafi, "A hybrid silicon-on-glass (SOG) lateral micro-accelerometer with CMOS readout circuitry," in *Proc. 15th IEEE MEMS Workshop*, Las Vegas, NV, Jan. 2002, pp. 623–626.

[16] T. Kinoshita, M. Hane, and J. P. McVittie, "Notching as an example of charging in uniform high density plasmas," *J. Vac. Sci. Technol. B, Microelectron. Process. Phenom.*, vol. 14, no. 1, pp. 560–565, Jan./Feb. 1996.

[17] T. Matsuura, M. Chabloz, J. Jiao, Y. Yoshida, and K. Tsutsumi, "A method to evade silicon backside damage in deep reactive ion etching for anodically bonded glass–silicon structures," *Sens. Actuators A, Phys.*, vol. 89, no. 1/2, pp. 71–75, Mar. 2001.

[18] C.-H. Kim, J. Park, N. Park, and Y.-K. Kim, "MEMS fiber-optic variable optical attenuator using collimating lensed fiber," in *Proc. IEEE/LEOS Int. Conf. Opt. MEMS*, Waikoloa, HI, Aug. 2003, pp. 145–146.

[19] *SiRRS01 Datasheet,* Silicon Sens., Plymouth, U.K., 2004. [Online]. Available: www.siliconsensing.com

[20] *SMG066 Product Information*, Robert Bosch GmbH, Gerlingen, Germany, 2001. [Online]. Available: www.bosch-sensortec.com

[21] *IDG-300 Product Information*, Invensense, Sunnyvale, CA, 2006. [Online]. Available: www.invensense.com

[22] *IEEE Standard Specification Format Guide and Test Procedure for Single-Axis Interferometric Fiber Optic Gyros*, IEEE Std 952-1997, 1998.

[23] *IEEE Standard Specification Format Guide and Test Procedure for Single-Axis Laser Gyros*, IEEE Std 647-1995, 1996.

Said Emre Alper was born in Ankara, Turkey, in 1976. He received the B.S., M.Sc., and Ph.D. degrees in electrical and electronics engineering (with high honors) from Middle East Technical University (METU), Ankara, in 1998, 2000, and 2005, respectively.

From 1998 to 2005, he was a Research Assistant with the MEMS-VLSI Research Group, Department of Electrical and Electronics Engineering, METU, where he has been a Senior Research Scientist since 2006. His major research interests include capacitive inertial sensors, micromachined resonators and actuators, capacitive interface circuits, and microfabrication technologies.

Dr. Alper received the "METU Thesis of the Year Award" in 2000 and 2005 for his M.Sc. thesis and Ph.D. dissertation, respectively, which were awarded by the Prof. Mustafa N. Parlar Education and Research Foundation. He is the first author of the symmetric and decoupled gyroscope design, which won the first-prize award in the operational designs category of the International Design Contest organized by DATE and CMP in March 2001. He is also the first author of the tactical-grade symmetrical and decoupled microgyroscope design, which won the third-prize award, among 132 MEMS designs from 24 countries and 25 states across the U.S., in the international 3-D MEMS Design Challenge organized by MEMGEN Corporation (currently Microfabrica), in June 2003.

Yuksel Temiz was born in Erzurum, Turkey, in 1982. He received the B.S. and M.S. degrees in electrical and electronics engineering from Middle East Technical University (METU), Ankara, Turkey, in 2005 and 2007, respectively, with the highest GPA among all graduates of the METU Engineering Faculty. He is currently working toward the Ph.D. degree with the Institute of Electrical Engineering, Ecole Polytechnique Fédérale de Lausanne (EPFL), Lausanne, Switzerland.

Between 2005 and 2007, he was a Research Assistant with the MEMS-VLSI Research Group, METU, with a full graduate fellowship provided by the Scientific and Technical Research Council of Turkey (TUBITAK). He is currently a Research/Teaching Assistant with the Microelectronic Systems Laboratory, EPFL. His research interests include readout and control electronics for micromachined inertial sensors, interface electronics for biosensors, and fabrication technologies for BioMEMS.

Tayfun Akin (S'90–M'97) was born in Van, Turkey, in 1966. He received the B.S. degree (with high honors) in electrical engineering from Middle East Technical University (METU), Ankara, Turkey, in 1987 and the M.S. and Ph.D. degrees in electrical engineering from the University of Michigan, Ann Arbor, in 1989 and 1994, respectively, with a graduate fellowship provided by the NATO Science Scholarship Program through the Scientific and Technical Research Council of Turkey (TUBITAK).

Beginning in 1995 and 1998, he was an Assistant Professor and an Associate Professor, respectively, with the Department of Electrical and Electronics Engineering, Middle East Technical University, where he has been a Professor since 2004. He is also the Director of the METU-MEMS Research Center, which has a 1300-m^2 clean-room area for MEMS process and testing. His research interests include MEMS, microsystems technologies, infrared detectors and readout circuits, silicon-based integrated sensors and transducers, and analog and digital integrated-circuit design.

Dr. Akin has served various MEMS, EUROSENSORS, and TRANSDUCERS conferences as a Technical Program Committee Member. He was the Cochair of the 19th IEEE International Conference of Micro Electro Mechanical Systems (MEMS 2006) held in Istanbul. He was the winner of the First Prize in the Experienced Analog/Digital Mixed-Signal Design Category at the 1994 Student VLSI Circuit Design Contest organized and sponsored by Mentor Graphics, Texas Instruments, Hewlett-Packard, Sun Microsystems, and Electronic Design Magazine. He is the coauthor of the symmetric and decoupled-gyroscope project that won the first-prize award in the operational designs category of the international design contest organized by the DATE Conference and CMP in March 2001. He is also the coauthor of the gyroscope project that won the third-prize award of the 3-D MEMS Design Challenge organized by MEMGen Corporation (currently Microfabrica).